Role of flexoelectric coupling in polarization rotations at the a-c domain walls in ferroelectric perovskites

Ye Cao[1], Long-Qing Chen[2], and Sergei V. Kalinin[1]

[1] Center for Nanophase Materials Sciences, Oak Ridge National Laboratory, Oak Ridge, TN 37831, USA

[2] Department of Material Sciences and Engineering, The Pennsylvania State University, University Park, PA 16802, USA

[Abstract]

Ferroelectric and ferroelastic domain walls play important roles in ferroelectric properties. However their couplings with flexoelectricity have been less understood. In this work we applied phase-field simulation to investigate the flexoelectric coupling with ferroelectric *a*/*c* twin structures in lead ziconate titanate (PZT) thin films. Local stress gradients were found to exist near twin walls that created both lateral and vertical electric fields through the flexoelectric effect, resulting in polarization inclinations from either horizontal or normal orientation, polarization rotation angles deviated from 90° and consequently highly asymmetric *a*/*c* twin walls. By tuning the flexoelectric strengths in a reasonable range from first-principle calculations, we found that the transverse flexoelectric coefficient has a larger influence on the polarization rotation than longitudinal and shear coefficients. As polar rotations that commonly occur at compositional morphotropic phase boundaries contribute to the piezoelectric enhancement, this work calls for further exploration of alternative strain-engineered polar rotations via flexoelectricity in ferroelectric thin films.

Flexoelectricity, a ubiquitous property in most insulating materials describes the coupling between electric polarization and strain gradient.[1, 2] Discovered several decades ago, flexoelectricity has long been neglected and less explored due to its small magnitude in bulk materials.[3] Recent development of nanoscale technology has aroused interests in flexoelectricity due to the enhanced strain gradients and flexoelectric strengths in nanoscale thin films. These include the measurement of flexoelectric coefficients via experimental approaches [4, 5] and first principles calculations[6, 7], the study of flexoelectric field induced mechanical switching [8-10], and the flexoelectric effect on ferroelectric domain patterning[11]. Large strain gradients are usually located near defect sites in ferroelectric thin films, such as oxygen vacancies, dislocations and domain walls, the latter of which has been long recognized to influence the ferroelectric properties. [12-14] Nevertheless the flexoelectric coupling with ferroelectric domain walls are less studied.[15, 16] Recently Catalan *et al*. observed polarization rotation in lead titanite ($PbTiO_3$) twined structure and attributed it to the flexoelectric effect.[17] However direct evidences associating polarization rotations with flexoelectricity are still lacking; partly due to the complexity and uncertainties of the flexoelectric coefficients. Thoughts then arise naturally about the threshold flexoelectric strength for experimentally observable polarization rotations, how does each component of the flexoelectric coefficient tensors affect the rotations separately, and whether we can determine the flexoelectric coefficients by comparing the theoretical calculations with experiments. These concerns can hardly be addressed from the perspective of experimental approach. Therefore we employed phase-field simulations[18] to study how flexoelectricity would influence the local strain/stress distribution, the polarization inclination and polarization rotations near *a*/*c* twin walls in ferroelectric thin films.

In the phase-field simulation of ferroelectric oxides, we take their paraelectric phase, which is typically of cubic symmetry as the reference state. The total free energy density of a ferroelectric crystal includes five energy contributions which are written as a function of polarization P_i, strain ε_{kl}, electric field E_i,and the gradient of P_i and ε_{kl},[19]

$$f = f_{land}(P_i) + f_{grad}(\nabla P_i) + f_{elast}(P_i, \varepsilon_{kl}) + f_{elec}(P_i, E_i) + f_{flexo}(P_i, \varepsilon_{kl}, \nabla P_i, \nabla \varepsilon_{kl}) \tag{1}$$

in which f_{land}, f_{grad}, f_{elast}, f_{elec} and f_{flexo} represent the Landau-Ginzburg-Devonshire (LGD) free energy density, the gradient energy density, the elastic energy density, the electrostatic energy density and the flexoelectric energy density respectively. The LGD free energy is written as a 6th order polynomial expansion of P_i,[20]

$$\begin{aligned} f_{land}(P_i) &= \alpha_i P_i^2 + \alpha_{ij} P_i^2 P_j^2 + \alpha_{ijk} P_i^2 P_j^2 P_k^2 \\ &= \alpha_1(T)\left(P_1^2 + P_2^2 + P_3^2\right) + \alpha_{11}\left(P_1^4 + P_2^4 + P_3^4\right) + \alpha_{12}\left(P_1^2 P_2^2 + P_2^2 P_3^2 + P_3^2 P_1^2\right) \\ &+ \alpha_{111}\left(P_1^6 + P_2^6 + P_3^6\right) + \alpha_{112}\left[P_1^2\left(P_2^4 + P_3^4\right) + P_2^2\left(P_1^4 + P_3^4\right) + P_3^2\left(P_1^4 + P_2^4\right)\right] + \alpha_{123} P_1^2 P_2^2 P_3^2 \end{aligned} \tag{2}$$

in which α are the landau coefficients and only α_1 is temperature dependent. The gradient energy is introduced through the polarization gradient,

$$\begin{aligned} f_{grad}(\nabla P_i) &= \frac{1}{2} g_{ijkl}\left(\frac{\partial P_i}{\partial x_j}\frac{\partial P_k}{\partial x_l}\right) \\ &= \frac{1}{2} g_{11}\left[\left(\frac{\partial P_1}{\partial x_1}\right)^2 + \left(\frac{\partial P_2}{\partial x_2}\right)^2 + \left(\frac{\partial P_3}{\partial x_3}\right)^2\right] + g_{12}\left(\frac{\partial P_1}{\partial x_2}\frac{\partial P_2}{\partial x_1} + \frac{\partial P_2}{\partial x_3}\frac{\partial P_3}{\partial x_2} + \frac{\partial P_3}{\partial x_1}\frac{\partial P_1}{\partial x_3}\right) \\ &+ \frac{1}{2} g_{44}\left[\left(\frac{\partial P_1}{\partial x_2} + \frac{\partial P_2}{\partial x_1}\right)^2 + \left(\frac{\partial P_2}{\partial x_3} + \frac{\partial P_3}{\partial x_2}\right)^2 + \left(\frac{\partial P_3}{\partial x_1} + \frac{\partial P_1}{\partial x_3}\right)^2\right] \end{aligned} \tag{3}$$

in which g_{ijkl} are the gradient energy coefficients. The elastic energy density is written as,[21]

$$f_{elas} = \frac{1}{2} c_{ijkl} (\varepsilon_{ij} - \varepsilon_{ij}^0)(\varepsilon_{kl} - \varepsilon_{kl}^0) \tag{4}$$

where c_{ijkl} is the elastic stiffness tensor, ε_{ij} is the total strain and ε_{ij}^0 is the eigenstrain induced by the spontaneous polarization P_i. To consider the dipole-dipole interaction during ferroelectric domain evolution, the electrostatic energy of a domain structure is introduced through,[22]

$$f_{elec}(P_i, E_i) = -P_i \left(E_i + \frac{E_i^d}{2} \right) = -\left(P_1 E_1 + P_2 E_2 + P_3 E_3 \right) - \frac{1}{2} \left(P_1 E_1^d + P_2 E_2^d + P_3 E_3^d \right) \tag{5}$$

where E_i and E_i^d are the applied electric field and depolarization field respectively. The flexoelectric energy density in Eq. (1) can be expanded as,[23]

$$f_{flexo}(P_i, \varepsilon_{kl}, \nabla P_i, \nabla \varepsilon_{kl}) = \frac{1}{2} f_{ijkl} \left(\frac{\partial P_k}{\partial x_l} \varepsilon_{ij} - \frac{\partial \varepsilon_{ij}}{\partial x_l} P_k \right) = \frac{1}{2} F_{ijkl} \left(\frac{\partial P_k}{\partial x_l} \sigma_{ij} - \frac{\partial \sigma_{ij}}{\partial x_l} P_k \right) \tag{6}$$

in which f_{ijkl} (unit: V) and F_{ijkl} (unit: Vm^2N^{-1}) are the flexocoupling coefficient (FCC) tensors, which are related through $f_{ijkl} = c_{ijmn} F_{mnkl}$. The driving force of P_i from the flexoelectric energy density is calculated through,

$$\frac{\delta f_{\text{flexo}}}{\delta P_k} = \frac{\partial f_{\text{flexo}}}{\partial P_k} - \frac{\partial}{\partial x_l} \frac{\partial f_{\text{flexo}}}{(\partial P_k / \partial x_l)} = -F_{ijkl} \frac{\partial \sigma_{ij}}{\partial x_l} = -E_k^f \tag{7}$$

where E_k^f is called the flexoelectric field (unit: V/m). It should be noted that although the flexoelectric field is very similar to the electric field, the latter of which is defined as the electrostatic driving force $\delta f_{\text{elec}} / \delta P_k = -E_k$, they are different in that the flexoelectric field only couples with polarization evolution and does not directly act on the space charge migration,

while electric field does both. For cubic symmetry the flexoelectric coefficient tensor has three independent components, i.e., F_{1111}, F_{1122} and F_{1221}.[24-26] By using Voigt notation $F_{11} = F_{1111}$, $F_{12} = F_{1122}$ and $F_{44} = 2F_{1221}$, Eq. (7) can be expanded as,

$$E_1^f = F_{11}\frac{\partial \sigma_1}{\partial x_1} + F_{12}\left(\frac{\partial \sigma_2}{\partial x_1} + \frac{\partial \sigma_3}{\partial x_1}\right) + F_{44}\left(\frac{\partial \sigma_5}{\partial x_3} + \frac{\partial \sigma_6}{\partial x_2}\right) \tag{8-1}$$

$$E_2^f = F_{11}\frac{\partial \sigma_2}{\partial x_2} + F_{12}\left(\frac{\partial \sigma_3}{\partial x_2} + \frac{\partial \sigma_1}{\partial x_2}\right) + F_{44}\left(\frac{\partial \sigma_6}{\partial x_1} + \frac{\partial \sigma_4}{\partial x_3}\right) \tag{8-2}$$

$$E_3^f = F_{11}\frac{\partial \sigma_3}{\partial x_3} + F_{12}\left(\frac{\partial \sigma_1}{\partial x_3} + \frac{\partial \sigma_2}{\partial x_3}\right) + F_{44}\left(\frac{\partial \sigma_4}{\partial x_2} + \frac{\partial \sigma_5}{\partial x_1}\right) \tag{8-3}$$

Finally the temporal evolution of the ferroelectric polarization is governed by the time-dependent LGD equations, [19]

$$\frac{\partial P_i(\boldsymbol{x},t)}{\partial t} = -L\frac{\delta F_{total}}{\delta P_i(\boldsymbol{x},t)}, i = 1,2,3, \tag{9}$$

in which $\boldsymbol{x}$ is the position, t is the time, L is the kinetic coefficient related to the domain movement, and $F_{total} = \int_V f dV$ is the total free energy.

In our simulations, we chose $Pb(Zr_{0.2}Ti_{0.8})O_3$ to preset the domain structure consisting of $(100)_a$ and $(001)_c$ domain variants as the model system (Fig. 1(a)). The film lies on the x-y plane with plane normal along z direction. The system is thus simplified into a two-dimensional (x-z) problem with a simulation size of $256\Delta x \times 64\Delta x$ and Δx =0.25nm. The thickness of the film and substrate are assumed to be $50\Delta x$ and $10\Delta x$, representing a 12.5nm thick thin film. A semi-implicit spectral method[27] was employed to solve the time-dependent LGD equation with

periodical boundary conditions applied along the *x* direction and thin film boundary condition along the *z* direction. The epitaxial substrate strain was set to be zero along *x* and *y* directions. The gradient energy coefficients are set to be $G_{11}/G_{110}=0.6$ while $G_{110}=1.73\times10^{-10}\mathrm{C^{-2}m^4N}$.[28] The flexocoupling coefficient (FCC) is chosen on the order of 10^{-11} $\mathrm{C^{-1}m^3}$ based on literature.[7] The Landau coefficients, electrostrictive coefficients and elastic compliance constants of $Pb(Zr_{0.2}Ti_{0.8})O_3$ are collected from literature[29-31]. The background dielectric constant of PZT is ε_r ≈5-7.[32, 33] However to compare with experimental results from real samples, we used ε_r of 50 as suggested from literature.[34]

The equilibrium PZT twin structure without the flexoelectric effect consisted of a majority of $(001)_c$ domain variants, as shown in Fig. 1(a). The polarization orientations in three typical zoom-in regions at different film depths near the *a*/*c* twin walls (indicated by colored boxes in 1(a) are represented by the arrow plots in Fig. 1 (b) ~ (d). On the top surface the polarization rotations are symmetric (1b) and the domain walls are well defined in the width of ~2.5nm. In the center (1c) and bottom layer (1d) of the film, the polarization rotations become sharper along one of the twin walls and smoother along the other, resulting in asymmetric twin walls with remarkable differences in wall widths. This is more clearly seen at the bottom surface, due to the substrate constraint at the film/substrate interface, which is gradually relaxed towards the top surface of the film. Notably the polarization orientations inside *a*/*c* domains remain horizontal/vertical away from the wall regions.

To investigate how the flexoelectric components (F_{11}, F_{12} and F_{44}) affect the PZT twin structure separately, we set F_{11}= 10 (10^{-11} $\mathrm{C^{-1}m^3}$) and kept F_{12} and F_{44} to be zero. Notably that due to the uncertainty of the magnitude of flexoelectric coefficients, we intentionally chose a larger F_{11} to enhance its effect, while a detailed discussion of the flexoelectric coefficient dependence

of the simulated behaviors will be provided later. The equilibrium polarization orientation near the twin walls at the bottom surface is illustrated in Fig. 2(a). In comparison with Fig. 1(d), the polarizations remained normal in the $(001)_c$ domain aside the left twin wall/substrate junction; however they tilted downward from the horizontal orientation in the $(100)_a$ domain. Thus the polarization rotation across the left twin wall is expected to be larger than 90˚. On the other hand, the polarizations in the $(100)_a$/$(001)_c$ domains near the right twin wall are substantially inclined from horizontal/vertical orientations, which renders the polarization rotations smaller than 90˚ across the right twin wall. An averaged one-dimensional (1D) plot of the out-of-plane polarization component (P_z) along the x direction (Fig. 3(a)) at different magnitude of F_{11} (= 0, 5, 10 (10^{-11} $C^{-1}m^3$)) shows that P_z's are ~0.6 (C/m^2) at different F_{11}'s in $(001)_c$ domains; however in $(100)_a$ domain P_z's decrease from 0 to -0.1 (C/m^2) with increasing F_{11}. This implies that the polarization inclination in the $(100)_a$ domain can be attributed to F_{11}.

To study the effect of the transverse flexoelectric strength on polarization orientations, we set F_{12}= 3.0 (10^{-11} $C^{-1}m^3$) and kept F_{11} and F_{44} to be zero. Unlike those in Fig. 2(a), the polarizations tilted towards $-x$ in the $(001)_c$ domain close to the left twin wall, and $+x$ in the $(001)_c$ domain close to the right twin wall. (Fig. 2(b)) In the $(100)_a$ domain the polarization vectors remained horizontal. All these are suggestive of polarization rotation deviations from 90˚ across the left/right twin walls. Fig. 3(b) shows 1D profiles of P_x's along the x direction at different F_{12}'s. When F_{12} increases, P_x's clearly decrease/increase in $(001)_c$ domains near left/right twin walls. We further studied the influence of shear flexoelectric strength by setting F_{44}= 10 (10^{-11} $C^{-1}m^3$) and kept F_{11} and F_{12} zero. From Fig. 2(c), the polarizations remained vertical in both $(001)_c$ domains and tilted towards +z in the $(100)_a$ domain. This tilt increases with increasing F_{44}'s, as evidenced by the P_z increase from 0 to 0.15 (C/m^2) in $(100)_a$ domain

(Figure 3(c)). As P_z's remained unchanged in $(001)_c$ domains at different F_{44}'s, the polarization rotation angles are expected to be less than 90° at both twin walls.

The polarization inclinations at the wall/bottom surface junctions are possibly due to the flexoelectric fields induced via local stress gradients. To verify it we demonstrated the stress distributions in PZT thin film with only longitudinal, transverse and shear flexoelectric strength as shown in Fig. 3(d) ~ (f). It is seen that local stresses are mostly concentrated in the vicinity of the twin walls at the bottom surface. In Fig. 3(d), the out-of-plane stress component (σ_3) at the junctions of bottom surface and left/right twin walls would induce pure downward/upward flexoelectric fields (E_3^f) based on Eq. (8-3), with (F_{11}, F_{12}, F_{44}) = (10, 0, 0) ($10^{-11}C^{-1}m^3$). This vertical E_3^f causes the horizontal polarization vectors in $(100)_a$ domain to tilt downward near the left wall and upward near the right wall, as illustrated in Fig. 2(a). On the other hand, σ_3 would also create in-plane flexoelectric fields (E_1^f) (Fig. 3(e)) when there is only transverse flexoelectric strength (F_{11}, F_{12}, F_{44}) = (0, 3, 0) ($10^{-11}C^{-1}m^3$) from Eq. (8-1). This in-plane E_1^f gives rise to polarization tilt towards –z and +z directions in $(001)_c$ domains (Fig. 2(b)). Finally when there is only shear flexoelectric strength (F_{11}, F_{12}, F_{44}) = (0, 0, 10) ($10^{-11}C^{-1}m^3$), the shear stress (σ_5) creates upward E_3^f based on Eq. (8-1), which macroscopically tilts horizontal polarization in $(100)_a$ domain towards +z direction (Fig. 2(c)). The stress distributions clearly explain the polarization inclination behaviors in Fig. 2(a) ~ (c).

We have therefore calculated the polarization rotation angles (θ) across left/right twin walls at different film depths as a function of longitudinal, transverse and shear flexoelectric

strength respectively (Fig.4 (a) ~ (c)). The rotation angle (θ) is calculated to be $\theta = \sum_i \theta_i$ where θ_i is the angle between two adjacent polarization vectors in the *x* direction,

$$\theta_i = P_i(P_x^i, P_y^i, P_z^i) \wedge P_{i+1}(P_x^{i+1}, P_y^{i+1}, P_z^{i+1}) = \cos^{-1} \frac{P_x^i P_x^{i+1} + P_y^i P_y^{i+1} + P_z^i P_z^{i+1}}{\sqrt{(P_x^i)^2 + (P_y^i)^2 + (P_z^i)^2}\sqrt{(P_x^{i+1})^2 + (P_y^{i+1})^2 + (P_z^{i+1})^2}} \quad (10)$$

and *i* ranges from $w_0 - w_d$ to $w_0 + w_d$ where w_0 is the center position of the domain walls and w_d is the half width of the domain walls. In Fig. 4(a), θ's across the top left and right twin walls (green solid and dashed lines) are equal to each other at F_{11}=0, and remain almost constant with increasing F_{11}. In the center of the film, the rotation angles become slightly larger than 90° at the left wall (blue solid line) and smaller than 90° at the right wall (blue dashed line), the difference between which are ~10° at different F_{11}'s. And the increase of θ with increasing F_{11} is almost negligible. However at the bottom surface of the film, θ across the left wall (red solid line) significantly increases with F_{11} and reaches ~107° at F_{11}=10 ($10^{-11}C^{-1}m^3$). On the other hand θ across the right wall (red dashed line) decrease to 75° at F_{11}=10 ($10^{-11}C^{-1}m^3$). The deviations of polarization rotation angles from 90° at the bottom surface are significantly larger than those at top surface and in the film center, signifying the remarkable polarization inclinations at the wall/bottom surface junctions.

The dependence of rotation angles on F_{12} is shown in Fig. 4(b). Similarly, the rotation angles θ on the top surface are almost equal to 90° at all F_{12}'s (green lines). In the center of the film θ's slightly deviate from 90° (blue lines) when F_{12} increases from 0 up to 3.0 ($10^{-11}C^{-1}m^3$). The twin walls become highly asymmetric near the bottom surface, as evidenced by the large

difference of θ's between left/right twin walls from 20° at F_{12}=0 up to 55° at F_{12}=3.0 ($10^{-11}C^{-1}m^3$). Notably the rotation angles increase/decrease exponentially with F_{12} at the bottom surface, compared to the linear dependence of θ on F_{11} (Fig. 4a). This indicates that the polarization rotations are more sensitive to F_{12} than F_{11}. To verify it we plotted the correlation factors $\delta=d(\text{Log }\theta)/d(\text{Log}F_{ij})$, i.e., the change of θ's with the change of F_{11} (F_{12})'s, as a function of F_{11} (F_{12}), which are illustrated in Fig. 4(d) and (e). At the bottom surface (red lines), the correlation factors of F_{12} are on the order of 10^{-1}, and reach 0.35 and -0.2 at F_{12}=3.0 ($10^{-11}C^{-1}m^3$), which is about 4 ~5 times larger than δ's at F_{11}=10 ($10^{-11}C^{-1}m^3$). In the top and center layer, δ's of F_{12} are also larger than those of F_{11}. Our simulation results indicate that F_{12} has a larger influence on polarization rotations than F_{11} does.

Finally we studied the dependence of rotation angles on F_{44} as shown in Fig. 4(c). While on the top and center layer θ's are relatively insensitive to the change of F_{44}, there is a decrease in θ's in the bottom layer at both left/right twin walls with increasing F_{44}. This is consistent with our previous simulation results that the vertical flexoelectric field from the shear stress globally tilts the horizontal polarizations towards +z direction in $(100)_a$ domain (Fig. 2(c)), resulting in polarization rotation angles less than 90° at both twin walls. The plot of correlation factor δ with F_{44} (Fig. 4(f)) further indicates that the effect of F_{44} on θ on top and center layer are negligible, and become significantly pronounced at the bottom surface. The values of δ reach -0.15 and -0.09 at F_{44}=10 ($10^{-11}C^{-1}m^3$), which implies that the influence of F_{44} on polarization rotations is slightly larger than F_{11}, but smaller than F_{12}.

While polarization rotations have been considered to be associated with piezoelectricity enhancement in compositionally engineered ferroelectrics near a morphotropic phase boundary, our simulation results imply that this polar rotation can also be generated in non-morphotropic

ferroelectrics via flexoelectricity facilitated strain engineering. The experimental characterization of polar rotation in $PbTiO_3$ was first reported by Catalan et. al, who attributed it to the flexoelectric effect.[17] Based on their observation and estimation, the flexo-induced polarization component $P_{(flexo)}$ could reach up to 0.15 C m^{-2}, and an average polar rotation angles of 10~15°. This agreed with our simulation results when F_{ij} reached ~$10^{-11}C^{-1}m^3$ (Fig. 3(a)~(c)). Interestingly only vertical polarization rotations in *c* domains were observed, while polar rotations in *a* domains are small, due to the in-plane flexoelectricity induced from horizontal gradient of vertical expansion ($d\varepsilon_3/dx_1$). In our phase-field simulation both vertical and horizontal polar rotations were seen, depending on the different combinations of flexoelectric coefficients, nevertheless the transverse coefficients were found to have a larger effect than the longitudinal and shear coefficients. Therefore comparisons between experimental observations of polarizations at the domain walls and theoretical calculations of all the flexoelectric coefficients and their effects on polar rotations allow us to reconstruct the flexoelectric coefficients of ferroelectric oxides. It should be noted that our model can readily be applied to other ferroelectric oxides without loss of generality, such as $BaTiO_3$ and $BiFeO_3$ with even higher flexoelectric responses.

In summary we applied the phase-field method to study the polarization rotation behaviors in $Pb(Zr_{0.2}Ti_{0.8})O_3$ thin films with *a*/*c* twined structures. Polarization inclinations from their original horizontal and vertical orientations have been observed, in both local and global manner, which are induced by the local stress gradients near the twin walls through flexoelectricity. A clear correlation between the degree of polarization rotation and each component of the flexoelectric coefficient tensor has been established, which implies that the transverse flexoelectric coefficient influences the rotations more profoundly. Our simulation

results thus offer an alternative method to determine the flexoelectric coefficients in ferroelectric thin films.

[Acknowledgement]

This study was supported by the U.S. DOE, Office of Basic Energy Sciences (BES), Materials Sciences and Engineering Division (MSED) through FWP Grant No. ERKCZ07 (Y.C., S.V.K.). A portion of this research was conducted at the Center for Nanophase Materials Sciences, which is a DOE Office of Science User Facility. L.Q.C is supported by the U.S. DOE, Office of BES, MSED under Award No. DE-FG02-07ER46417.

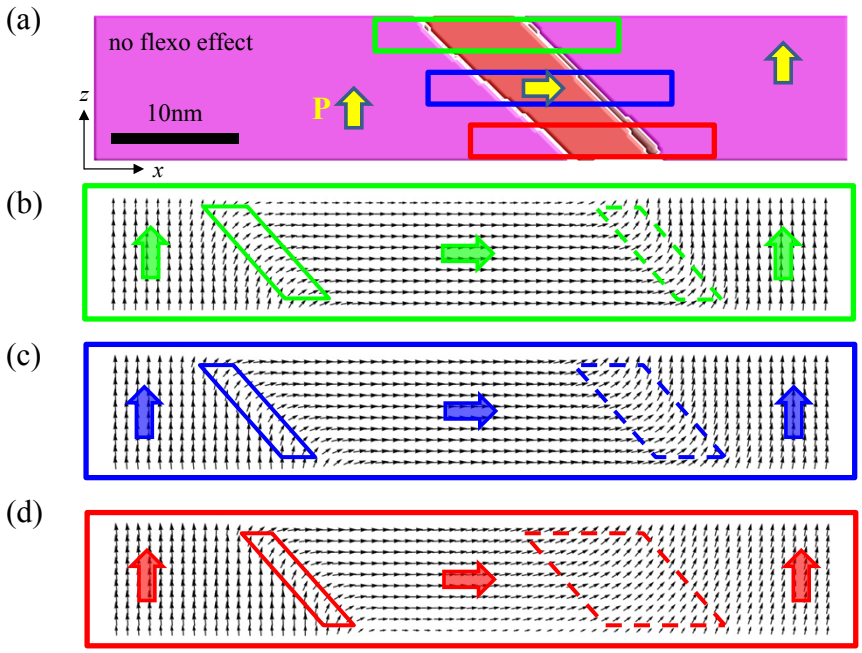

Fig. 1 (a) 2D (x-z plane) $(100)_a/(001)_c$ domain structure in 12.5nm thick $Pb(Zr_{0.2}Ti_{0.8})O_3$ thin film without flexoelectric effect, and polarization vector plots near the twin wall regions at the top (b), center (c) and bottom layers (d) of the film marked by the colored solid boxes in (a). The arrows in (a) ~ (d) illustrate the polarization orientations and the rhomboids in (b) ~ (d) indicate the twin wall regions.

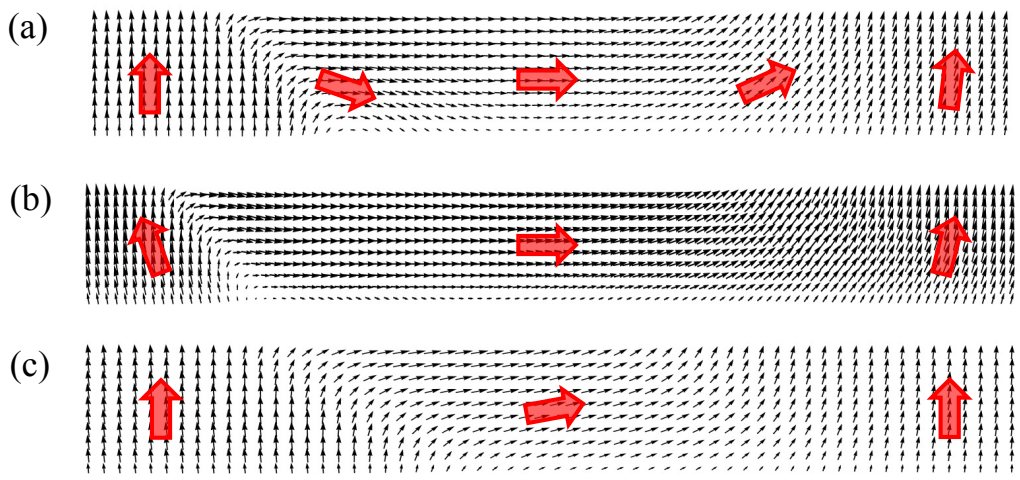

Fig. 2 2D (*x*-*z* plane) plot of polarization vectors in the vicinity of twin walls at the bottom surface of the film (marked by red solid box in Fig. 1(a)) with only (a) longitudinal flexoelectric coefficient F_{11}=10, F_{12}= F_{44}=0; (b) transverse flexoelectric coefficient F_{12}=3.0, F_{11}= F_{44}=0; and (c) shear flexoelectric coefficient F_{44}=10, F_{11}= F_{12}=0. The red arrows indicate the local polarization orientations. (unit of F_{ij}: $10^{-11}C^{-1}m^3$)

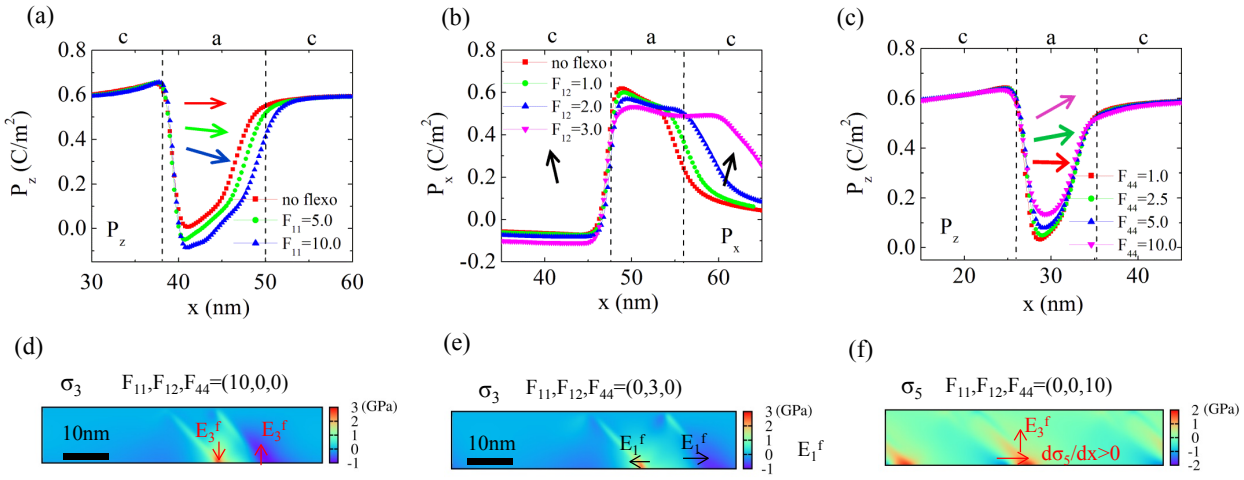

Fig. 3 (a) ~ (c) 1D profile (along x near bottom surface) of polarization component (P_x, P_z) across a/c twin walls at different magnitudes of (a) longitudinal (F_{11}), (b) transverse (F_{12}) and (c) shear (F_{44}) flexoelectric coefficients. Arrows indicate inclinations of both in-plane and out-of-plane polarizations. (d) ~ (f) 2D (x-z plane) normal (σ_3) and shear stress (σ_5) distributions in the entire thin film when (d) F_{11}=10, F_{12}= F_{44}=0, (e) F_{12}=3.0, F_{11}= F_{44}=0, (f) F_{44}=10, F_{11}= F_{12}=0. The arrows indicate the local flexoelectric field induced by the stress gradients through flexoelectricity. (unit of F_{ij}: $10^{-11}C^{-1}m^3$)

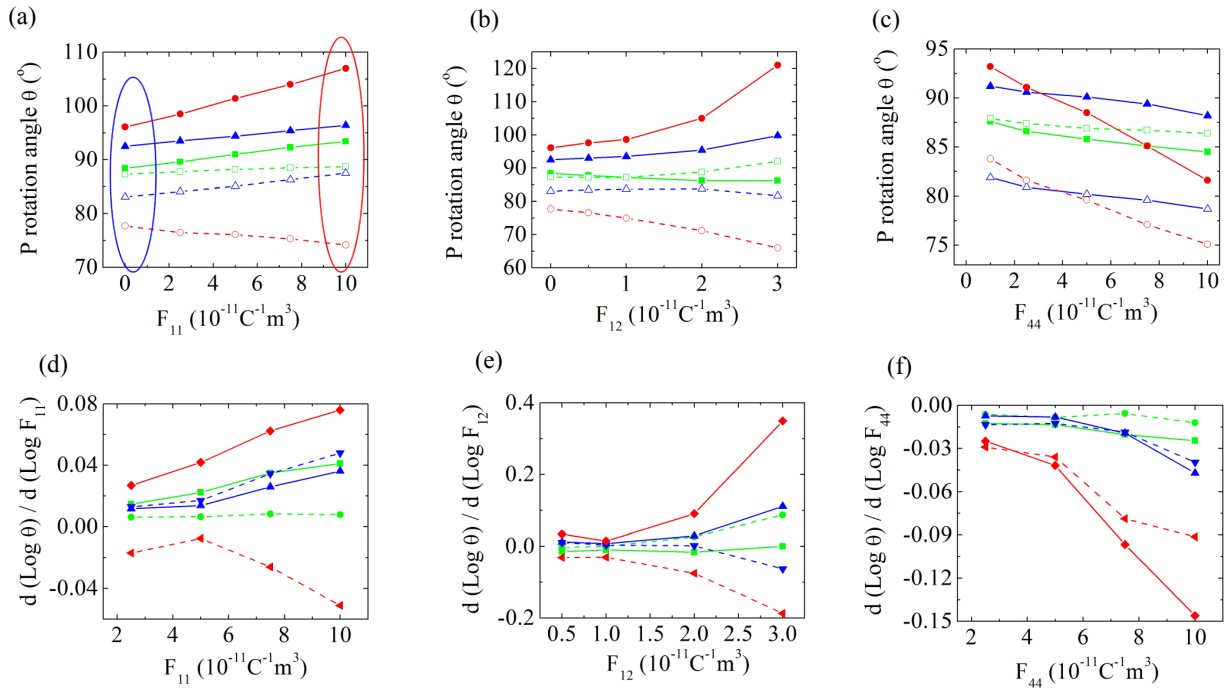

Fig. 4 Dependence of (a) ~ (c) polarization rotation angles (θ) and (d) ~ (f) correlation factors $\delta=d(\text{Log }\theta)/d(\text{Log}F_{ij})$ as a function of (a, d) longitudinal (F_{11}), (b, e) transverse (F_{12}) and (c, f) shear (F_{44}) flexoelectric coefficients. Green, blue and red lines represent the twin walls along the top, center and bottom layers respectively, while solid and dashed lines denote the left and right twin walls in all the figures.

[References]

1. P. V. Yudin and A. K. Tagantsev, Nanotechnology **24** (43) (2013).
2. P. Zubko, G. Catalan and A. K. Tagantsev, Annual Review of Materials Research, Vol 43 **43**, 387-421 (2013).
3. S. M. Kogan, Soviet Physics-Solid State **5** (10), 2069-2070 (1964).
4. W. H. Ma and L. E. Cross, Applied Physics Letters **86** (7), 072905 (2005).
5. W. H. Ma and L. E. Cross, Applied Physics Letters **82** (19), 3293-3295 (2003).
6. J. W. Hong, G. Catalan, J. F. Scott and E. Artacho, Journal of Physics-Condensed Matter **22**, 112201 (2010).
7. J. W. Hong and D. Vanderbilt, Physical Review B **88**, 174107 (2013).
8. H. Lu, C. W. Bark, D. E. de los Ojos, J. Alcala, C. B. Eom, G. Catalan and A. Gruverman, Science **336** (6077), 59-61 (2012).
9. Y. J. Gu, Z. J. Hong, J. Britson and L. Q. Chen, Applied Physics Letters **106**, 022904 (2015).
10. J. Ocenasek, H. Lu, C. W. Bark, C. B. Eom, J. Alcala, G. Catalan and A. Gruverman, Physical Review B **92**, 035417 (2015).
11. R. Ahluwalia, A. K. Tagantsev, P. Yudin, N. Setter, N. Ng and D. J. Srolovitz, Physical Review B **89**, 174105 (2014).
12. J. Seidel, L. W. Martin, Q. He, Q. Zhan, Y. H. Chu, A. Rother, M. E. Hawkridge, P. Maksymovych, P. Yu, M. Gajek, N. Balke, S. V. Kalinin, S. Gemming, F. Wang, G. Catalan, J. F. Scott, N. A. Spaldin, J. Orenstein and R. Ramesh, Nature Materials **8** (3), 229-234 (2009).
13. P. Maksymovych, J. Seidel, Y. H. Chu, P. P. Wu, A. P. Baddorf, L. Q. Chen, S. V. Kalinin and R. Ramesh, Nano Letters **11** (5), 1906-1912 (2011).
14. A. Tselev, P. Yu, Y. Cao, L. R. Dedon, L. W. Martin, S. V. Kalinin and P. Maksymovych, Nat Commun **7** (2016).
15. P. V. Yudin, A. K. Tagantsev, E. A. Eliseev, A. N. Morozovska and N. Setter, Physical Review B **86**, 134102 (2012).
16. Y. J. Gu, M. L. Li, A. N. Morozovska, Y. Wang, E. A. Eliseev, V. Gopalan and L. Q. Chen, Physical Review B **89**, 174111 (2014).
17. G. Catalan, A. Lubk, A. H. G. Vlooswijk, E. Snoeck, C. Magen, A. Janssens, G. Rispens, G. Rijnders, D. H. A. Blank and B. Noheda, Nature Materials **10** (12), 963-967 (2011).
18. L. Q. Chen, Annu Rev Mater Res **32**, 113-140 (2002).
19. L. Q. Chen, Journal of the American Ceramic Society **91** (6), 1835-1844 (2008).
20. Y. L. Li, S. Y. Hu, Z. K. Liu and L. Q. Chen, Applied Physics Letters **78** (24), 3878-3880 (2001).
21. Y. L. Li, S. Y. Hu, Z. K. Liu and L. Q. Chen, Acta Materialia **50** (2), 395-411 (2002).
22. Y. L. Li, L. Q. Chen, G. Asayama, D. G. Schlom, M. A. Zurbuchen and S. K. Streiffer, Journal of Applied Physics **95** (11), 6332-6340 (2004).
23. Y. J. Gu, The Pennsylvania State University, 2014.
24. H. Le Quang and Q. C. He, Proceedings of the Royal Society a-Mathematical Physical and Engineering Sciences **467** (2132), 2369-2386 (2011).
25. L. L. Shu, X. Y. Wei, T. Pang, X. Yao and C. L. Wang, Journal of Applied Physics **110**, 104106 (2011).
26. L. L. Shu, X. Y. Wei, T. Pang, X. Yao and C. L. Wang, Journal of Applied Physics **116**, 129901 (2014).
27. L. Q. Chen and J. Shen, Computer Physics Communications **108** (2-3), 147-158 (1998).
28. F. Xue, J. J. Wang, G. Sheng, E. Huang, Y. Cao, H. H. Huang, P. Munroe, R. Mahjoub, Y. L. Li, V. Nagarajan and L. Q. Chen, Acta Materialia **61** (8), 2909-2918 (2013).
29. M. J. Haun, Z. Q. Zhuang, E. Furman, S. J. Jang and L. E. Cross, Ferroelectrics **99**, 45-54 (1989).

30. M. J. Haun, E. Furman, S. J. Jang, H. A. Mckinstry and L. E. Cross, Journal of Applied Physics **62** (8), 3331-3338 (1987).
31. M. J. Haun, E. Furman, S. J. Jang and L. E. Cross, Ferroelectrics **99**, 13-25 (1989).
32. A. K. Tagantsev, G. Gerra and N. Setter, Physical Review B **77** (17), 174111 (2008).
33. A. N. Morozovska, E. A. Eliseev, S. V. Svechnikov, A. D. Krutov, V. Y. Shur, A. Y. Borisevich, P. Maksymovych and S. V. Kalinin, Physical Review B **81** (20), 205308 (2010).
34. G. Rupprecht and R. O. Bell, Physical Review **135** (3A), A748 (1964).